Recent Developments on Polymeric Membranes for CO_2 Capture from Flue Gas

Yang Han [†], *W.S. Winston Ho* [†,‡,*]

[†] William G. Lowrie Department of Chemical and Biomolecular Engineering, The Ohio State University, 151 West Woodruff Avenue, Columbus, OH 43210-1350, USA

[‡] Department of Materials Science and Engineering, The Ohio State University, 2041 College Road, Columbus, OH 43210-1178, USA

* Corresponding author. Tel.: +1 614 292 9970; fax: +1 614 292 3769.

E-mail address: ho.192@osu.edu (W.S.W. Ho).

Abstract: Polymeric membranes have been widely considered as one of the next-generation technologies for CO_2 capture from fossil fuel-derived flue gases. This separation modality requires novel polymeric materials that possess efficient CO_2/N_2 separation properties, as well as chemical and mechanical stability for a multiyear membrane lifetime. In this paper, recent developments in polymeric membranes tailored for post-combustion carbon capture are reviewed. The selected polymeric materials encompass ether oxygen-rich polymers, polynorbornenes, ionic liquid membranes, and facilitated transport membranes. In each of the selected materials, noteworthy research efforts for material design and membrane formation are highlighted. The performances of the selected materials are compared in the CO_2/N_2 selectivity-CO_2 permeance plot. As the only class of materials reviewed herein that have demonstrated the fabrication of thin-film composite membranes in scale, facilitated transport membranes have shown both high selectivity and permeance at relevant conditions for post-combustion carbon capture. However, comprehensive field tests are needed to resolve the technical gap between the material development and the commercial application.

Nomenclature

A_D	fitting parameter in diffusivity-free volume correlation
B_D	fitting parameter in diffusivity-free volume correlation
FFV	fractional free volume
J	gas permeation flux through membrane
ℓ	effective membrane thickness
P	gas permeability
Δp	partial pressure differential across membrane
S	gas solubility in membrane
D	gas diffusivity in membrane

Greek letters

α	ideal selectivity

Subscripts

i	gaseous species i
j	gaseous species j

1. Introduction

In 2018, the Intergovernmental Panel on Climate Change (IPCC) drafted a special report on the economical and sociological impacts of global warming of 1.5°C in the context of greenhouse gas emissions [1]. The report highlights the urgent need for sustainable low-carbon development pathways, and the mitigation of carbon emissions is regarded as the vital measure for limiting the global warming. In the U.S., the electric power sector emitted 1,763 million tonnes of CO_2 in 2018, 65% of which stemmed from the combustion of coal [2]. Considering the tremendous carbon footprint, the U.S. Department of Energy has been sponsoring a wide variety of projects to decarbonize coal-derived flue gases [3]. The flue gases are typically discharged at atmospheric pressure containing 11 – 15 vol.% CO_2 [4]. The low CO_2 partial pressure, along with the enormous volumetric flow rate, constitutes great technical challenge for efficient CO_2/N_2 separation [5, 6].

Polymeric membrane is an emerging technology in the pursuit of low-carbon power generation. It is a thin polymeric interphase that acts as a CO_2-selective barrier, which separates the CO_2-lean flue gas and the CO_2-rich permeate. Compared to other CO_2 separation methods, polymeric membrane is advantageous for its system compactness, energy efficiency, system flexibility for dynamic operations, and ability to overcome thermodynamic solubility limitations [7]. Nearly hundreds of new polymeric materials have been reported in the past decade with the ability to promote the fast permeation of CO_2 versus N_2 [8, 9]. However, a fundamental barrier is the permeability-selectivity trade-off, that is, highly permeable polymers tend to possess less selectivity and *vice versa* [10]. Robeson first proposed an empirical upper bound in 1991 to describe such a limiting behavior [11]. The design of better polymers that surpass the Robeson upper bound, therefore, has been the main theme of membrane research.

In 2018, we published a review paper with a focus on the promising polymeric materials for energy-intensive CO_2 separations [12]. The research efforts to shift the corresponding upper bounds were also discussed, including the enhanced CO_2 solubility in ether oxygen-rich polymers, the size sieving ability in novel shape-persisting polymers, and the carrier-mediated CO_2 permeation in facilitated transport membranes. Despite of our goal of being comprehensive and perspective, a few classes of important polymers were not included in our previous review. In addition, noteworthy progress has been achieved in the synthesis of CO_2-philic rubbery polymers and facilitated transport membranes. Therefore, an update on these recent developments is necessary.

In this review, the gas transport mechanisms through polymeric membranes are discussed first as background information. Research highlights in ether oxygen-rich polymers, polynorbornenes, ionic liquid membranes, and facilitated transport membranes are then reviewed with focuses on structure–property relationships and potential for industrial applications.

2. Gas Permeation in Polymers

2.1. Solution-diffusion mechanism

Membrane separation is a pressure-driven process. The light-gas penetrants firstly dissolve in the membrane on the high-pressure side, diffuse down the chemical potential gradient, and desorb to the low-pressure side. This conceptual model is termed as the solution-diffusion mechanism, which is well-adopted to describe the gas permeation in non-reactive polymers. Under this scheme, the flux of a penetrant (J_i) is proportional to its transmembrane partial pressure differential (Δp_i). The proportionality, which is related to the mass transfer resistance, is defined as the permeance (P_i/ℓ)

$$\frac{P_i}{\ell} = \frac{J_i}{\Delta p_i} \quad (1)$$

The permeance is expressed in Gas Permeation Unit (GPU, 1 GPU = 1×10^{-6} cm^3(STP) cm^{-2} s^{-1} $cmHg^{-1}$). Gas permeability coefficient (P_i), the intrinsic characteristic of the gas permeation process, can then be calculated by multiplying the permeance with the membrane thickness (ℓ). Since the solvation and diffusion steps are both thermally activated processes, the permeability coefficient can be further expressed as the product of the solubility coefficient (S_i) and the diffusion coefficient (D_i) [13, 14]

$$P_i = S_i \times D_i \tag{2}$$

The permeability data are commonly reported in the unit of Barrer (1 Barrer = 1×10^{-10} cm^3(STP) cm cm^{-2} s^{-1} $cmHg^{-1}$). The permeability is an intrinsic property of the polymer, whereas the permeance dependents on the thickness and configuration of the membrane formed by the polymer.

The intrinsic separation characteristic of the membrane is measured by the ideal selectivity (α_{ij}), which is the ratio of two gas permeabilities. The ideal selectivity can be further expressed as the product of solubility selectivity (S_i/S_j) and diffusivity selectivity (D_i/D_j)

$$\alpha_{ij} = \frac{S_i}{S_j} \times \frac{D_i}{D_j} \tag{3}$$

Therefore, the separation arises from the difference in solubilities or diffusivities of the gas pair in the polymer. The sorption of a gas penetrant in a polymer is often enthalpy-driven, where the heat of sorption depends on the condensability of the gas and the affinity of the gas to the polymer. Two common measures for the condensability are the critical temperature and Lennard-Jones temperature of the gas [14-16]. These values for CO_2 and N_2 are summarized in Table 1. As shown, CO_2 exhibits a higher condensability than N_2, which translates to a favorable CO_2 solubility selectivity over N_2 in most polymers. The CO_2/N_2 solubility selectivity can be further enhanced

by introducing CO_2-philic functional groups in the polymer. This feature has been heavily exploited by a class of rubbery polymer containing high content of ether oxygen [15-18].

The sorption behavior results in the occupancy of voids in the polymer by the penetrant. The penetrant can then migrate into a void above a critical size by random volume fluctuation [19]. The gas diffusivity in a weakly interacting polymer is correlated to the fractional free volume (FFV) according to [20]

$$D_i = A_D \cdot \exp\left(-\frac{B_D}{\mathrm{FFV}}\right) \tag{4}$$

where the front factor A_D and the parameter in the exponential term B_D are both related to the kinetic size of the penetrant. The kinetic diameters and critical volumes of CO_2 and N_2 are also summarized in Table 1. CO_2 has a smaller kinetic diameter but a larger critical volume than those of N_2. Therefore, the diffusivity selectivity might favor CO_2 but typically not to the extent that allows for efficient CO_2/N_2 separation. For this reason, most high free volume glassy polymers rely on the CO_2–polymer interaction to exhibit certain selectivity.

2.2. Facilitated transport mechanism

Facilitated transport membranes feature reactive polymers that are capable of a reversible reaction with CO_2 [21]. Figure 1 shows a schematic of gas permeation in a facilitated transport membrane [22]. As seen, the CO_2 carrier can either be functional groups that are covalently bound to the polymer backbone or freely mobile moieties that are confined in the polymer matrix. The former is termed as the fixed-site carrier and the latter is the mobile carrier [23]. Like the solution-diffusion mechanism, the gaseous penetrants also need to dissolve in the polymer, but at least one of them (e.g., CO_2) should be able to form a reaction product with the carrier in the membrane on the high-pressure side. Driven by the concentration gradient, the reaction product can migrate either by the intramolecular diffusion though the neighboring carrier sites in the fixed-site carrier,

or by the intermolecular diffusion of the mobile carrier product through the polymer matrix. On the low-pressure side, the reaction product decomposes, releases the CO_2, and regenerates the carrier. It should be noted that the reactive diffusion scheme does not exclude the solution-diffusion of unreacted CO_2 molecules. In most cases, the overall CO_2 flux through the membrane is expressed as

$$J_{CO_2} = \frac{P_{CO_2}}{\ell}\Delta p_{CO_2} + \frac{P_{\text{carrier-}CO_2}}{\ell}\Delta p_{\text{carrier-}CO_2} \quad (5)$$

where the first and second terms on the right-hand side of the equation represent the fluxes of Fickian diffusion and reactive diffusion, respectively. The carrier-mediated diffusion enhances the permeation of CO_2. Contrarily, other light gases that are non-reactive to the carrier can only permeate based on the solution-diffusion mechanism, and their fluxes are typically a few orders of magnitude lower than that of CO_2 [24].

The seemingly straightforward expression in Eq. (5) is notoriously difficult to analyze in a facilitated transport membrane with a complex reaction network. For instance, $p_{\text{carrier-}CO_2}$ in Eq. (5) is the gas-phase equivalent partial pressure of the CO_2-carrier complex. It is related to the CO_2 partial pressure in the gas phase in accordance with the physisorption and chemisorption of CO_2 in the reactive polymer [25]. Consequently, the overall CO_2 permeability in a facilitated transport membrane is not a constant (compared to Eq. (1)), but a function of the CO_2 partial pressure and the membrane thickness [26, 27]. Specifically, the sorption and desorption of CO_2 occur through the reversible CO_2-carrier reaction at the membrane-gas interfaces. These interfacial reactions impose additional mass transfer resistances, which are independent on the membrane thickness. Consequently, the CO_2 permeability typically reduces with decreasing membrane thickness. For this reason, the transport properties of CO_2 through facilitated transport membranes are commonly reported in terms of CO_2 permeance at specific feed and permeate conditions. CO_2 permeability

data are also available in the literature, but a cautious interpretation is required since a high CO_2 permeability of a micron-thick film does not guarantee an equivalently high CO_2 permeance in a thin-film composite membrane.

3. Membranes Based on Solution-Diffusion Mechanism

3.1. Ether oxygen-rich polymers

A CO_2 molecule has a sizable quadrupole moment due to the electron-deficient carbon center [28]. It is known that the polar ethylene oxide group (–C–C–O–) or ether linkage (–C–O–C–) possesses a high affinity to CO_2 via the quadrupole-quadrupole interaction. Due to the uneven distribution of charges inside the molecules, the carbon atom carries partial positive charge while the oxygen atoms carry partial negative charges. The CO_2 molecules tend to align such that their oxygen atoms are near the positively charged regions of the polymer and their carbon atoms are near the negatively charged regions of the polymer, thus providing a strong net attraction. Therefore, a high CO_2 solubility can be achieved by the preferential interaction, and polymers with high content of ether oxygen are of great interest for CO_2/N_2 separation. Liu et al. studied the binding geometries and energies between CO_2 and oligomers with various ether oxygen contents by density functional theory [29]. Three substrates were investigated in their study: nonane (O:C = 0), diethylene glycol dimethyl ether (diglyme) (O:C = 0.5), and 1-methoxy-2-(methoxymethoxy)ethane (TOO) (O:C = 0.6). As shown in Figure 2, increasing the oxygen-to-carbon ratio results in a higher binding energy with CO_2, thereby an enhanced absorption of CO_2. However, polymers containing a high content of ether oxygen are known to exhibit high crystallinity [30]. One example is semi-crystalline poly(ethylene oxide) (PEO), which has a moderate O:C ratio of 0.5 but a low CO_2 permeability of 12 Barrers [18]. The low permeability stems from the limited gas diffusivity in the semi-crystalline regions.

Various methods have been reported to suppress the formation of semi-crystalline regions in PEO-based polymers. Important approaches include (1) block copolymerization with bulky, hard segment, (2) blending with low MW ether to disrupt chain packing, and (3) crosslinking to form branched polymer [12]. However, several new polymers with ether functionality have been reported recently, featuring improved CO_2/N_2 separation performance or advanced understanding of the polymer nanostructure. The CO_2 permeabilities and CO_2/N_2 selectivities of these new materials are summarized in Table 2 based on the synthesis strategies.

A new class of ether oxygen-rich polymer has been synthesized by using heterocyclic acetals. The heterocyclic acetal reacts with an alkoxy acrylate to induce the ring opening of the acetal, which effectively grafts an ether-containing linkage onto the vinyl substrate. Afterwards, a photo-polymerization step polymerizes the monomers and results in a vinyl polymer with ether oxygen-rich side chains. A poly(1,3-dioxolane) has been reported by Liu et al. with a high O:C ratio of 0.67 [29]. A low glass transition temperature (T_g) below –60°C was observed for the polymer, indicating the successful synthesis of CO_2-philic rubber. As shown in Figure 3, the high O:C ratio bestowed the polymer a high CO_2 permeability of 1400 Barrers and a CO_2/N_2 selectivity of 64 at 70°C. Compared to other PEO-based polymers, this new polymer exhibited an unprecedently high CO_2/N_2 selectivity at an elevated temperature, which can be attractive since no flue gas cooling is required [7].

A variation of this polymer has been reported by the same group, where 1,3,5-trioxane was used as the cyclic acetal and an O:C ratio of 0.8 was achieved [31]. Unfortunately, the high ether oxygen content led to a low fractional free volume, thereby a reduced CO_2 permeability. A series of block copolymers was also synthesized with various ratios of 1,3-dioxolane and 1,3,5-trioxane.

The transport measurements confirmed that the CO_2 permeability reduced from 232 to 52 Barrers at 50°C with increasing O:C ratio from 0.66 to 0.74.

A method complementary to the synthesis of new ether-containing polymers is to copolymerize the soft ether segment with a rigid segment. Common choices of the rigid segment include aromatic amide, aromatic imide, and styrene [12]. Recently, Karunakaran et al. have synthesized a series of polyacrylonitrile-*r*-poly(ethylene glycol) methyl ether methacrylate (PAN-*r*-PEGMA) copolymers via free radical polymerization, and a thin selective layer was dip-coated on a PAN support [32]. The soft PEGMA segment provided the CO_2 affinity while the PAN hard segment disrupted the polymer chain packing. By increasing the fraction of PAN, the composite membranes showed a 35-fold increase in the CO_2 permeability with the highest CO_2/N_2 selectivity of 65 at 25°C. It was claimed by the authors that the PAN-containing copolymers were soluble in solvents that were non-invasive to the PAN support, which benefited the composite membrane synthesis. Akhtar et al. further extended this concept and synthesized an amphiphilic random copolymer poly(acrylonitrile-*r*-PEGMA-*r*-*N*,*N*-dimethyl amino ethyl acrylate) (PAN-*r*-PEGMA-*r*-PDMAEMA)) [33]. Compared to the PAN-*r*-PEGMA copolymer, the DMAEMA unit contained a tertiary amino group, which was affinitive to CO_2 and H_2O. Therefore, the tercopolymer demonstrated a CO_2 permeability of 47 Barrers and a high CO_2/N_2 selectivity of 67 in the presence of water vapor at 25°C.

Aside from PAN, Kline et al. employed a triptycene-containing linear polyimide as the hard segment to block copolymerize with crosslinked PEO [34]. The relatively long chain PEO segments entwined with the polyimide, forming semi-interpenetrating polymer networks (s-IPNs). By increasing the length of the PEO segment, the CO_2 permeability increased by nearly 66%, with the highest CO_2 permeability of 90 Barrers and a CO_2/N_2 selectivity of 46 at 35°C. Another s-IPN

was reported by Kim et al., utilizing poly(glycidyl methacrylate-*g*-polypropylene glycol)-*co*-poly(oxyethylene methacrylate) (PGP-POEM) to intercalate with Pebax®-1657 [35]. Due to the higher ether oxygen content, this s-IPN showed a higher CO_2 permeability of 237 Barrers with a CO_2/N_2 selectivity of 39 at 35°C.

Another noticeable advancement in refraining the crystallinity of PEO is by crosslinking with amino functional polyhedral oligomeric silsesquioxanes (POSS-NH_2) [36]. It was reported that the incorporation of POSS-NH_2 not only promoted the gas diffusion, but also enhanced the impregnation of low MW poly(ethylene glycol) (PEG). Therefore, a high CO_2 permeability of 1567 Barrers with a CO_2/N_2 selectivity of 69 was obtained at 35°C.

3.2. Polynorbornenes

Norbornene, a bridged cyclic hydrocarbon, can be polymerized and produce different macromolecular structures depending on the choice of catalyst [37]. Norbornene can undergo ring-opening metathesis polymerization (ROMP) to form cyclolinear unsaturated polymers [38]. Alternatively, vinyl-addition polymerization can also occur, resulting in bulky bicyclic repeating units without unsaturated bonds as shown in Figure 4 [39]. These polynorbornenes are highly glassy, but did not catch much attention in the membrane society due to their relatively low gas permeabilities. However, researchers recently introduced alkoxy silyl pendant groups into the norbornene monomers, producing novel polymers with high free volume and better affinity to CO_2. The CO_2 permeabilities and CO_2/N_2 selectivities of noteworthy polynorbornenes are summarized in Table 3 based on the synthesis strategies.

The simplest silylation treatment of the norbornene monomer is by substituting the H on the ε position of norbornene with a trimethylsilyl group (–$Si(Me)_3$). A homopolymer of poly(trimethylsilyl norbornene) (PNB-$Si(Me)_3$) has been synthesized by Maroon et al. and

demonstrated a high CO_2 permeability of 4371 Barrers but a low CO_2/N_2 selectivity of 13 at 35°C [40]. The transport results are consistent with other advanced polymers with high free volume, where the size-sieving ability is insufficient to yield efficient CO_2/N_2 separation.

In order to further improve the CO_2/N_2 selectivity, the trimethylsilyl substituent has been replaced by a series of alkoxy silyl groups with various contents of ether oxygen. Gmernicki et al. have reported mono- to tri-substituted PNB-Si(Me)$_3$ by ethoxy group (–OEt) [41]. The incorporation of the polar but soft pendant groups led to a reduction in the CO_2 permeability but an improved CO_2/N_2 selectivity. For instance, the bi-substituted counterpart showed a reduced CO_2 permeability of 474 Barrers with a higher selectivity of 19.3.

As detailed in Section 3.1, increasing the O:C ratio benefits the CO_2/N_2 solubility selectivity in ether oxygen-rich polymers. A similar approach has been reported by Maroon et al. using 2-methoxyethoxy (–OEtOMe) to further enhance the polarity of the silyl pendant groups [40]. As shown in Figure 5, random copolymers of PNB-Si(OEt)$_3$-Si(OEtOMe)$_3$ with different ethoxy-to-methoxymethoxy ratios have been synthesized. Increasing the methoxymethoxy content reduced the stiffness of the polymer chain but enhanced the CO_2 solubility. This trade-off led to the best CO_2/N_2 selectivity of 27.5 with a CO_2 permeability of 733 at a 50:50 monomer blending ratio.

Aside from the norbornene-derived polymers, tricyclononenes with three fused rings have also been utilized for polymer synthesis as shown in Figure 4. Due to the extra ring structure in the polymer backbone, these macromolecules are termed as Janus tricyclononene polymers. Like the polynorbornene counterpart, alkoxy silyl groups were grafted as side groups to enhance the CO_2/N_2 solubility selectivity. Alentiev et al. have prepared polymers with alkoxy silyl groups of different lengths (Me, Et, *n*-Pr, *n*-Bu) [42]. The bulky *n*-Bu substituent led to a high CO_2

permeability of 1100 Barrers with a CO_2/N_2 selectivity of 16.2. It should be noted that all polymers with alkoxy silyl groups may suffer from physical ageing.

Another variation that has been reported was to polymerize 5-vinyl-2-norbornene. The two alkene functionalities in the monomer resulted in a highly crosslinked polymer network bearing rigid fused ring structures [43]. This polyvinylnorbornene featured a better size-sieving ability than other polynorbornenes, evidenced by its decent CO_2/N_2 selectivity of 21.7 at 35°C. However, the crosslinking also reduced the free volume of the polymer and led to a lower CO_2 permeability of 104 Barrers.

3.3. Ionic Liquid Membranes

Ionic liquids (ILs) are organic salts that exhibit liquid-like properties at ambient temperature. Due to the strong ionic strength, ILs are known to have low vapor pressures and good thermal stability. Various IL-based membranes have been developed for CO_2/N_2 separation, and these membranes typically possess high CO_2/N_2 solubility selectivities [44]. A common issue of IL-based membranes are the processing and membrane formation. The incorporation of ILs in a membrane can weaken its mechanical properties, which limits the formation of thin-film composite membranes [45]. In order to overcome this issue, various methods to host a high content of ILs have been developed, including (1) crosslinked ion-gel membranes, (2) poly(ionene)s, and (3) poly(ionomer)s as shown in Figure 6. The CO_2 permeabilities and CO_2/N_2 selectivities of selected IL-containing membranes are summarized in Table 4 based on the synthesis strategies. Recent research highlights of these three categories will be discussed below.

The first approach to formulate a mechanically robust IL-containing membrane is to use a highly crosslinked rubbery polymer to host the ILs. The blending of the polymer and ILs is typically performed prior to the crosslinking, resulting in an ion-gel mixture with good film-

forming ability. Branched PEO is the most common host for ILs. It has been reported that the incorporation of ILs can plasticize these polymers and significantly enhance the CO_2 permeability [46]. Deng et al. developed a method to photo-polymerize poly(ethylene glycol) diacrylate (PEGDA) and tris(2-aminoethyl)amine (TAEA) to form a crosslinked polymer network with low crystallinity as shown in Figure 7 [47]. A variety of ILs containing 1-butyl-3-methylimidazolium ($[bmim]^+$) and different anions were incorporated, and the best anion identified was bis(trifluoromethane)sulfonimide ($[Tf_2N]^-$), showing a high CO_2 permeability of 135 Barrers and a CO_2/N_2 selectivity of 45.3 at 35°C. Different from the Michael addition scheme between amine and acrylate, Kusuma et al. photo-polymerized ethoxylated trimethylolpropane triacrylate, a monomer with a 20:3 ethylene glycol/acrylate ratio, and 3,6-dioxa-1,8-octanethiol [48]. This thiol-Michael addition featured faster kinetics and led to a highly crosslinked PEO network. They also incorporated a variety of $[Tf_2N]$-based ILs to form ion-gel membranes. The best cation, 1-ethyl-3-methylimidazolium ($[emim]^+$), demonstrated a CO_2 permeability of 529 Barrers and a CO_2/N_2 selectivity of 30.8 at 40°C. A variation of the previous approach was to use a thiol-decorated polysiloxane as reported by Kusuma et al. [49]. The resultant PEO-siloxane copolymer showed a better miscibility with ILs and yielded a relatively high CO_2/N_2 selectivity of 54 at 40°C. The crosslinking density and the chain length of the ethoxylated acrylate were also studied to correlate the gel configurations to the yield strengths of the membranes [46]. A gel network that was prone to plasticization generally exhibited a higher CO_2 permeability, but the improved transport properties were not necessarily accompanied by a higher yield strength.

The previous gel networks themselves do not bear any ionic species. However, several research groups have developed methods to incorporate the ionic groups directly onto the polymer. The various efforts can be categorized into two motifs: (1) poly(ionene)s and (2) poly(ionomer)s.

Poly(ionene)s have the cation or anion directly in the polymer backbone, while ionic functional groups present as pedant groups in poly(ionomer)s.

Bara and coworkers have devised several poly(ionene)s, which consist of imidazolium-containing polyimide (see Figure 8) [50] and Tröger's base-containing diimidazole ([Im-TB(*o*)-C_{10}]$^+$) [51]. These polymers intrinsically were not limited by the ionic content and not subject to nanoscale phase separation at a high IL content. However, the rigid polymer backbone generally led to a limited CO_2 permeability below 20 Barrers. A recent work by Yin et al. utilized the Debus-Radziszewski reaction to synthesize an amino-terminated imidazolium monomer coupled with $[Tf_2N]^-$ as the counterion [52]. Glycidyl ether crosslinkers were then added to form a rubbery poly(ionene) network. After blending with [emim][Tf_2N], the membrane exhibited a considerable CO_2 permeability of 2070 Barrers and a decent CO_2/N_2 selectivity of 24.6 at 35°C. Attributed to the highly flexible polymer chains, a higher crosslinking degree was reported to improve both the CO_2 diffusivity and solubility.

Compared to poly(ionene)s, the chemistry employed for poly(ionomer)s synthesis has shown a greater deal of variety. Ito et al. synthesized a sulfonated polyimide blended with 1-butyl-3-methylimidazolium bis(trifluoromethane)sulfonimide ([C_4mim][Tf_2N]) [53]. The IL plasticized the glassy polymer and formed bi-continuous nanostructures. These factors resulted in a CO_2 permeability of 431 Barrers and a CO_2/N_2 selectivity of 30 at 30°C. Nexar, a midblock-sulfonated polystyrene, was also used to host [bmim][BF_4] [54]. In the presence of water vapor, the membrane showed a decent CO_2 permeability of 153 Barrers but a relatively high CO_2/N_2 selectivity of 64 at 35°C. Another poly(ionomer) of interest is pyrrolidinium polycation ([HPyr]$^+$) paired with cyano-functionalized anions, such as $[C(CN)_3]^-$, $[N(CN)_2]^-$, and $[B(CN)_4]^-$ [55, 56].

The use of cyano-derivatives generally led to a better CO_2/N_2 selectivity, with the highest value of 61 at 20°C.

4. Facilitated Transport Membranes

4.1. Amine-containing membranes

The most exploited carriers to formulate CO_2-selective facilitated transport membranes are amines. The reaction mechanisms of CO_2 with different types of amines are briefly discussed below. CO_2 can serve as a Lewis acid that undergoes nucleophilic addition reaction with a Lewis base. Most primary and secondary amines can react with the electrophilic carbonyl center of CO_2 to form a zwitterion as shown in Eq. (6). A rapid intramolecular proton transfer can occur in the zwitterion, and the resultant carbamic acid is readily deprotonated by another amine to afford carbamate and ammonium ions as shown in Eq. (7). Overall, 2 moles of amine are needed for 1 mole of CO_2.

$$CO_2 + R–NH_2 \rightleftharpoons R–NH_2^+–COO^- \rightleftharpoons R–NH–COOH \quad (6)$$

$$R–NH–COOH + R–NH_2 \rightleftharpoons R–NH–COO^- + R–NH_3^+ \quad (7)$$

At a lower pH, the carbamate species can be hydrolyzed to produce bicarbonate and release a free amine [57]. However, the hydrolysis reaction is not favorable due to the decent stability of the carbamate.

A sterically hindered amine reacts with CO_2 differently. A sterically hindered amine is either a primary amine where the amino group is attached to a tertiary carbon or a secondary amine in which the amino group is attached to at least a secondary or tertiary carbon [58]. If the amine is hindered, the carbamate is unstable and prone to hydrolysis, resulting in the formation of bicarbonate and the regeneration of the amine:

$$CO_2 + R_1–NH–R_2 \rightleftharpoons R_1R_2–NH^+–COO^- \rightleftharpoons R_1R_2–N–COOH \quad (8)$$

$$R_1R_2\text{–N–COOH} + R_1\text{–NH–}R_2 \rightleftharpoons R_1R_2\text{–N–COO}^- + R_1R_2\text{–NH}_2^+ \quad (9)$$

$$R_1R_2\text{–N–COO}^- + H_2O \rightleftharpoons R_1\text{–NH–}R_2 + HCO_3^- \quad (10)$$

Overall, 1 mole of sterically hindered amine can fixate 1 mole of CO_2. Therefore, sterically hindered amines are advantageous over conventional amines for CO_2 capture due to their high CO_2 loading capacity [59, 60]. However, bulky substituents surrounding the amino group also retard its reaction kinetics with CO_2 [59]. The choice of amine, therefore, greatly affects the CO_2/N_2 separation properties of the facilitated transport membranes.

The CO_2 permeances and CO_2/N_2 selectivities of selected amine-containing facilitated transport membranes are summarized in Table 5. As discussed in Section 2.2, the CO_2 permeability of a facilitated transport membrane depends on the CO_2 partial pressure and the membrane thickness. It is generally invalid to speculate the permeance of a thin-film composite facilitated transport membrane based on the permeability data obtained from a thick film. For practical reasons, the CO_2 permeances, rather than the permeabilities, are listed in Table 5. In accordance, the thicknesses of the selective layers are also provided.

Han and coworkers have synthesized several amino acid salts as the mobile carriers to enhance the CO_2 permeation through a polyvinylamine (PVAm) matrix [61]. α-aminoacids, including glycine (Gly) and sarcosine (Sar), were deprotonated by a cyclic multi-amine, 2-(1-piperazinyl)ethylamine (PZEA) to form involatile aminoacid salts with high amine contents. Due to the organic cation, these aminoacids are miscible with the aminopolymer up to 85 wt.%. This feature enabled the coating of 170-nm selective layer on a nanoporous polyethersulfone support, and the composite membrane exhibited a CO_2 permeance of 839 GPU and a high CO_2/N_2 selectivity of 161 at 57°C. The high selectivity at an elevated operating temperature also avoided the need for flue gas cooling. The membranes were also tested extensively under mild feed gas

compression as well as a vacuum down to 0.2 atm on the permeate side [62]. It has been shown that the CO_2 permeance exhibited a strong dependence on the permeate vacuum. A high vacuum degree dehydrated the water-swellable polymer matrix, while a low vacuum degree retarded the desorption of CO_2 on the permeate side. The effect of temperature on the CO_2/N_2 separation was also studied. A higher temperature enhanced the permeations of both CO_2 and N_2. However, N_2 exhibited a higher activation energy of permeation than that of CO_2. An excessively high temperature benefited the CO_2 permeance but inevitably reduced the CO_2/N_2 selectivity. Because of this trade-off, the optimal performance was achieved at 67°C with a CO_2 permeance of 1450 GPU and a CO_2/N_2 selectivity of 165.

The same research group has also demonstrated the scalable fabrication of the thin-film composite membrane, which was rolled into prototype spiral-wound membrane modules with a membrane area up to 1.4 m^2 [63]. The membrane modules were tested at the National Carbon Capture Center, Wilsonville, Alabama, U.S.A. with actual flue gas slipstream containing 2 ppm SO_2 and 7.6% O_2. As shown in Figure 9, despite of the multiple flue gas outages, the membrane modules demonstrated 500-h stable operation with transport performance comparable to the flat-sheet membrane.

A similar method has been reported by Dai et al., where Gly, proline (Pro), and cystine (Cys) were deprotonated by KOH to form aminoacid salts as mobile carriers in hollow-fiber membranes [64]. After blended with poly(vinyl alcohol) (PVA), potassium prolinate (Pro-K) showed the highest CO_2 permeance of 793 GPU with a CO_2/N_2 selectivity of 40 at room temperature. The lower selectivity was caused likely by the lower operating temperature and the associated lower water partial pressure in the feed gas. Once again, the scalability of facilitated transport membrane enabled the fabrication of hollow-fiber membrane modules, and a field test was conducted using

petroleum coke-fired flue gas generated from a rotary kiln in Gubbio, Italy [65]. The long-term stability was also studied through a test for a duration of one week. Fly ash fouling was reported to adversely affect the membrane stability, indicating the importance of flue gas pre-treatment.

Aside from the synthesis of new mobile carriers, efforts to tune the structural properties of the hosting polymer were also reported. Janakiram et al. dispersed surface-modified nanocellulose in PVA to enhance the water cluster retention in the polymer matrix [66]. With the incorporation of sterically hindered polyamine as the fixed-site carrier and PZEA-Sar as the mobile carrier, thin-film composite membranes were synthesized, and a CO_2 permeance of 652 GPU with a CO_2/N_2 selectivity of 41 was obtained at 35°C. More importantly, a forced break test was conducted to study the membrane stability under humidity fluctuation. As shown in Figure 10, the incorporation of nanocellulose mitigated the impact of the dry-wet cycles, thereby improving the membrane stability.

4.2. Other carriers

Although most research activities in facilitated transport membranes concern the tuning of amine structures, other types of CO_2 carriers featuring different CO_2 chemistry were also reported. Arginine (Arg), an α-aminoacid containing a protonated guanidium ion, has been used as mobile carrier in PVA [64] and carboxymethylated nanocellulose [67]. Noticeably, the addition of Arg in nanocellulose led to a CO_2 permeability of 220 Barrers with a high CO_2/N_2 selectivity of 185 at 35°C, which significantly changed the gas transport performance of cellulose-based membranes. Park et al. studied the interaction of potassium trifluoroacetate (CF_3CO_2K) with water by nuclear magnetic resonance (NMR) [68]. The ^1H NMR results indicated that water could bound to the metal ion, resulting in extremely exposed hydrogen atoms to serve as Lewis acids to interact with the electronegative oxygen atoms in CO_2. By blending the salt into PEO, 1.3-μm thick composite

membranes were fabricated. In the presence of water vapor, the membrane exhibited a very high CO_2 permeance of 4650 GPU and a CO_2/N_2 of 1500. Noteworthily, the CO_2 permeance was extremely sensitive to the feed pressure. A slightly increased feed pressure from 1.01 to 1.05 bar resulted in an 82% loss of the CO_2 permeance. The severe susceptibility to carrier saturation imposes operational challenges in a practical gas separation process.

5. Conclusions

The recent developments in polymeric membranes for post-combustion carbon capture were reviewed. To compare the various polymeric membrane materials, selected data from Tables 2 – 5 are plotted in Figure 11, along with the 2008 Robeson upper bound [69]. In order to compare with the permeance data of the facilitated transport membranes, the permeability data of the solution-diffusion membranes are converted to their corresponding permeances assuming a 100-nm thick selective layer in a thin-film composite membrane. In addition, the possible mass transfer resistance from the polymer support is not considered. Admittedly, the transformation of a polymeric material into a thin-film composite membrane is non-trivial. The permeance data of the solution-diffusion membranes herein are sheerly a projection of their potential. Also plotted in Figure 11 as grey cross markers are the CO_2/N_2 separation performance of selected polymeric materials reviewed in our previous paper [12]. As seen, the advanced materials discussed in this review have shown significant improvement on the CO_2/N_2 selectivity, evidenced by the various ionic liquid membranes and ether oxygen-rich polymers approaching to the highly selective end of the upper bound. This advancement is not surprising since the gas permeation in these polymers is regulated by their solubility selectivities. On the other hand, the highly glassy polynorbornenes generally exhibited advantages in CO_2 permeance but suffered from a lack of CO_2/N_2 selectivity.

For this reason, the recent research work of introducing CO_2-philic functional groups in polynorbornenes might be promising to improve their selectivity.

Bestowed by their excellent CO_2/N_2 selectivities, facilitated transport membranes have exhibited separation performance above the upper bound. As the only class of materials reviewed herein that have demonstrated the fabrication of thin-film composite membranes in scale, facilitated transport membranes have shown CO_2 permeances above 1000 GPU at relevant conditions for post-combustion carbon capture. Comprehensive field tests in bench and pilot scales are needed to resolve the technical gap between the material development and the deployment in commercial-scale gas separations.

Acknowledgments

We would like to thank David Lang and José Figueroa of the Department of Energy-National Energy Technology Laboratory for providing helpful discussion and input. We would like to gratefully acknowledge the U.S. Department of Energy-National Energy Technology Laboratory (DE-FE0026919) and the Ohio Development Services Agency (OOE-CDO-D-13-05 and OER-CDO-D-15-09) for their financial support of this work. This work was partly supported by the Department of Energy under Award Number DE-FE0026919 with substantial involvement of the National Energy Technology Laboratory, Pittsburgh, PA, USA.

References

[1] Allen M, Babiker M, Chen Y, de Coninck H, Conors S. *Global Warming of 1.5 °C: An IPCC Special Report on the Impacts of Global Warming of 1.5 °C above Pre-industrial Levels and Related Global Greenhouse Gas Emission Pathways, in the Context of Strengthening the Global Response to the Threat of Climate Change, Sustainable Development, and Efforts to Eradicate Poverty*, Intergovernmental Panel on Climate Change: Incheon, Republic of Korea, 2018.

[2] U.S. Energy Information Administration, *Electricity Generation and Consumption*. https://www.eia.gov/electricity/data.php (accessed August 16, 2019).

[3] Figueroa JD, Fout T, Plasynski S, McIlvried H, Srivastava RD. *Int. J. Greenh. Gas Con.* 2008, 2, 9–20.

[4] Black J. *Cost and Performance Baseline for Fossil Energy Plants Volume 1: Bituminous Coal and Natural Gas to Electricity Final report*, 2nd, National Energy Technology Laboratory, November, 2010.

[5] Zhao L, Riensche E, Blum L, Stolten D. *Energy Procedia* 2011, 4, 629–636.

[6] Zhao L, Riensche E, Blum L, Stolten D. *J. Membr. Sci.* 2010, 359, 160–172.

[7] Ramasubramanian K, Zhao Y, Ho WSW. *AIChE J.* 2013, 59, 1033–1045.

[8] Wang S, Li X, Wu H, Tian Z, Xin Q, He G, Peng D, Chen S, Yin Y, Jiang Z. *Energy Environ. Sci.* 2016, 9, 1863–1890.

[9] Du N, Park HB, Dal-Cin MM, Guiver MD. *Energy Environ. Sci.* 2012, 5, 7306–7322.

[10] Robeson L, Freeman B, Paul D, Rowe B. *J. Membr. Sci.* 2009, 341, 178–185.

[11] Robeson LM. *J. Membr. Sci.* 1991, 62, 165–185.

[12] Han Y, Ho WSW. *Chin. J. Chem. Eng.* 2018, 26, 2238–2254.

[13] Wijmans J, Baker R. *J. Membr. Sci.* 1995, 107, 1–21.

[14] Ho WSW, Sirkar KK. *Membrane Handbook*, Chapman & Hall, New York, 1992, Kluwer Academic Publishers, Boston, reprint edition, 2001.

[15] Lin H, Freeman BD. *J. Mol. Struct.* 2005, 739, 57–74.

[16] Bondar V, Freeman B, Pinnau I. *J. Polym. Sci. Part B: Polym. Phys.* 2000, 38, 2051–2062.

[17] Lin H, Freeman BD. *Macromolecules* 2005, 38, 8394–8407.

[18] Lin H, Freeman BD. *J. Membr. Sci.* 2004, 239, 105–117.

[19] Freeman BD. *Macromolecules* 1999, 32, 375–380.

[20] Thran A, Kroll G, Faupel F. *J. Polym. Sci. Part B: Polym. Phys.* 1999, 37, 3344–3358.

[21] Goddard JD, Schultz JS, Suchdeo SR. *AIChE J.* 1974, 20, 625–645.

[22] Zhao Y, Ho WSW. *Ind. Eng. Chem. Res.* 2012, 52, 8774–8782.

[23] Cussler E, Aris R, Bhown A. *J. Membr. Sci.* 1989, 43, 149–164.

[24] Tong Z, Ho WSW. *Sep. Sci. Technol.* 2017, 52, 156–167.

[25] Schultz JS, Goddard JD, Suchdeo SR. *AIChE J.* 1974, 20, 417–445.

[26] Ansaloni L, Zhao Y, Jung BT, Ramasubramanian K, Baschetti MG, Ho WSW. *J. Membr. Sci.* 2015, 490, 18–28.

[27] Noble RD. *J. Membr. Sci.* 1992, 75, 121–129.

[28] Rindfleisch F, DiNoia TP, McHugh MA. *J. Phys. Chem.* 1996, 100, 15581–15587.

[29] Liu J, Zhang S, Jiang D, Doherty CM, Hill AJ, Cheng C, Park HB, Lin H. *Joule* 2019, 3, 1881–1894.

[30] Zhu L, Mimnaugh BR, Ge Q, Quirk RP, Cheng SZ, Thomas EL, Lotz B, Hsiao BS, Yeh F, Liu L. *Polymer* 2001, 42, 9121–9131.

[31] Liu J, Zhang G, Clark K, Lin H. *ACS Appl. Mater. Interfaces* 2019, 11, 10933–10940.

[32] Karunakaran M, Kumar M, Shevate R, Akhtar F, Peinemann K-V. *Polymers* 2017, 9, 219.

[33] Akhtar FH, Kumar M, Vovusha H, Shevate R, Villalobos LF, Schwingenschlögl U, Peinemann K-V. *Macromolecules* 2019,

[34] Kline GK, Zhang Q, Weidman JR, Guo R. *J. Membr. Sci.* 2017, 544, 143–150.

[35] Kim NU, Park BJ, Park MS, Park JT, Kim JH. *Chem. Eng. J.* 2019, 360, 1468–1476.

[36] Li S, Jiang X, Yang X, Bai Y, Shao L. *J. Membr. Sci.* 2019, 570, 278–285.

[37] Bermeshev MV, Syromolotov AV, Gringolts ML, Starannikova LE, Yampolskii YP, Finkelshtein ES. *Macromolecules* 2011, 44, 6637–6640.

[38] Boyle BM, Heinz O, Miyake GM, Ding Y. *Macromolecules* 2019, 3426−3434.

[39] Alentiev DA, Egorova ES, Bermeshev MV, Starannikova LE, Yampolskii YP, Finkelshtein ES. *Polym. Eng. Sci.* 2019, 1.

[40] Maroon CR, Townsend J, Gmernicki KR, Harrigan DJ, Sundell BJ, Lawrence III JA, Mahurin SM, Vogiatzis KD, Long BK. *Macromolecules* 2019, 52, 1589–1600.

[41] Gmernicki KR, Hong E, Maroon CR, Mahurin SM, Sokolov AP, Saito T, Long BK. *ACS Macro Letters* 2016, 5, 879–883.

[42] Alentiev DA, Egorova ES, Bermeshev MV, Starannikova LE, Topchiy MA, Asachenko AF, Gribanov PS, Nechaev MS, Yampolskii YP, Finkelshtein ES. *J. Mater. Chem. A* 2018, 6, 19393–19408.

[43] Dujardin W, Van Goethem C, Steele JA, Roeffaers M, Vankelecom IF, Koeckelberghs G. *Polymers* 2019, 11, 704.

[44] Cowan MG, Gin DL, Noble RD. *Acc. Chem. Res.* 2016, 49, 724–732.

[45] Kasahara S, Kamio E, Yoshizumi A, Matsuyama H. *Chem. Commun.* 2014, 50, 2996–2999.

[46] Kusuma VA, Chen C, Baker JS, Macala MK, Hopkinson D. *Polymer* 2019, 180, 121666.

[47] Deng J, Yu J, Dai Z, Deng L. *Ind. Eng. Chem. Res.* 2019, 58, 5261–5268.

[48] Kusuma VA, Macala MK, Baker JS, Hopkinson D. *Ind. Eng. Chem. Res.* 2018, 57, 11658–11667.

[49] Kusuma VA, Macala MK, Liu J, Marti AM, Hirsch RJ, Hill LJ, Hopkinson D. *J. Membr. Sci.* 2018, 545, 292–300.

[50] Mittenthal MS, Flowers BS, Bara JE, Whitley JW, Spear SK, Roveda JD, Wallace DA, Shannon MS, Holler R, Martens R. *Ind. Eng. Chem. Res.* 2017, 56, 5055–5069.

[51] Kammakakam I, O'Harra KE, Bara JE, Jackson EM. *ACS Omega* 2019, 4, 3439–3448.

[52] Yin J, Zhang C, Yu Y, Hao T, Wang H, Ding X, Meng J. *J. Membr. Sci.* 2019, in press.

[53] Ito A, Yasuda T, Yoshioka T, Yoshida A, Li X, Hashimoto K, Nagai K, Shibayama M, Watanabe M. *Macromolecules* 2018, 51, 7112–7120.

[54] Dai Z, Ansaloni L, Ryan JJ, Spontak RJ, Deng L. *J. Membr. Sci.* 2019, 117193.

[55] Teodoro RM, Tomé LC, Mantione D, Mecerreyes D, Marrucho IM. *J. Membr. Sci.* 2018, 552, 341–348.

[56] Tomé LC, Guerreiro DC, Teodoro RM, Alves VD, Marrucho IM. *J. Membr. Sci.* 2018, 549, 267–274.

[57] Danckwerts P. *Chem. Eng. Sci.* 1979, 34, 443–446.

[58] Sartori G, Savage DW. *Ind. Eng. Chem. Fundam.* 1983, 22, 239–249.

[59] Zhao Y, Ho WSW. *J. Membr. Sci.* 2012, 415, 132–138.

[60] Tong Z, Ho WSW. *J. Membr. Sci.* 2017, 543, 202–211.

[61] Han Y, Wu D, Ho WSW. *J. Membr. Sci.* 2018, 567, 261–271.

[62] Han Y, Wu D, Ho WSW. *J. Membr. Sci.* 2019, 573, 476–484.

[63] Han Y, Salim W, Chen KK, Wu D, Ho WSW. *J. Membr. Sci.* 2019, 575, 242–251.

[64] Dai Z, Deng J, Ansaloni L, Janakiram S, Deng L. *J. Membr. Sci.* 2019, 578, 61–68.

[65] Dai Z, Fabio S, Marino NG, Riccardo C, Deng L. *Int. J. Greenh. Gas Con.* 2019, 86, 191–200.

[66] Janakiram S, Yu X, Ansaloni L, Dai Z, Deng L. *ACS Appl. Mater. Interfaces* 2019, 11, 33302–33313.

[67] Venturi D, Chrysanthou A, Dhuiège B, Missoum K, Giacinti Baschetti M. *Nanomaterials* 2019, 9, 877.

[68] Park SC, Chae IS, Moon GH, Kim BS, Jang J, Wessling M, Kang YS. *J. Mater. Chem. A* 2019, 5190–5194.

[69] Robeson LM. *J. Membr. Sci.* 2008, 320, 390–400.

Figures

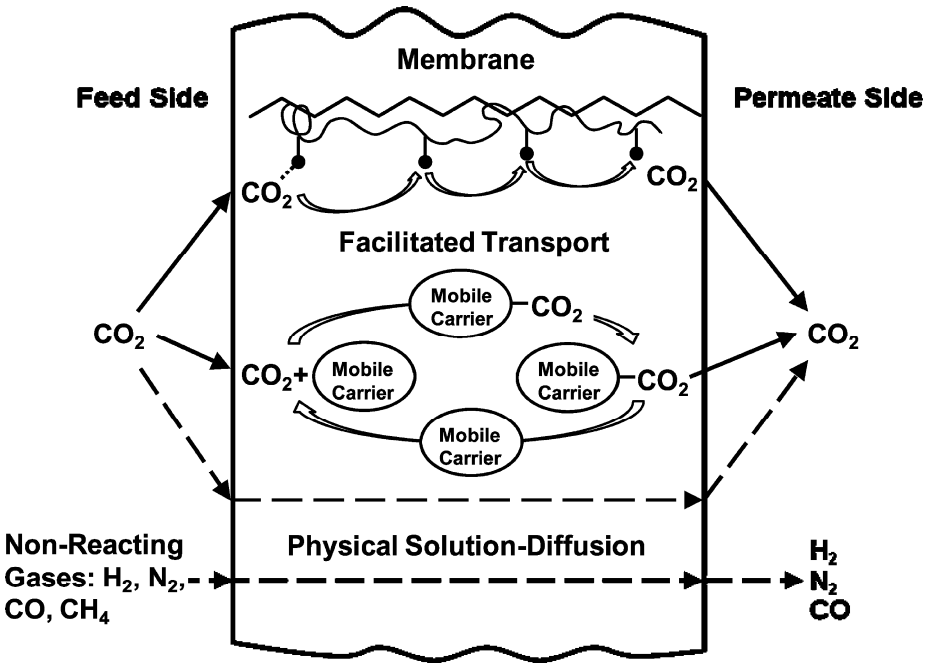

Figure 1. Schematic of gas permeation through a facilitated transport membrane. Adapted from Ref. [22] with permission from American Chemical Society (ACS).

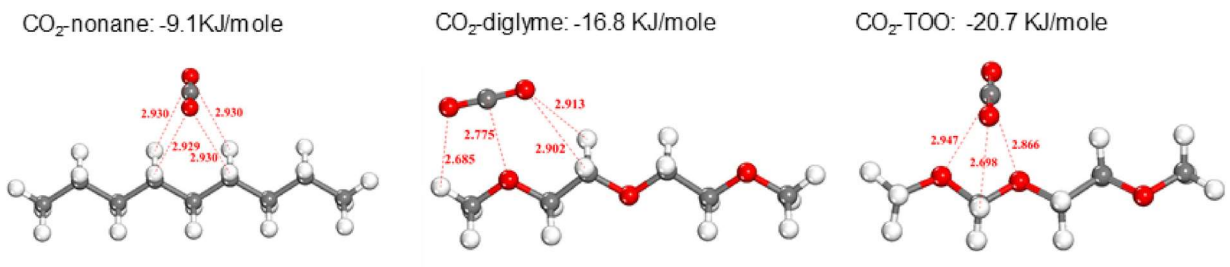

Figure 2. Binding geometries and energies of CO_2 and oligomers with various ether oxygen contents. Bond lengths are in the unit of Å. Key: C, gray; O, red; H, white. Adapted from Ref. [29] with permission from Elsevier.

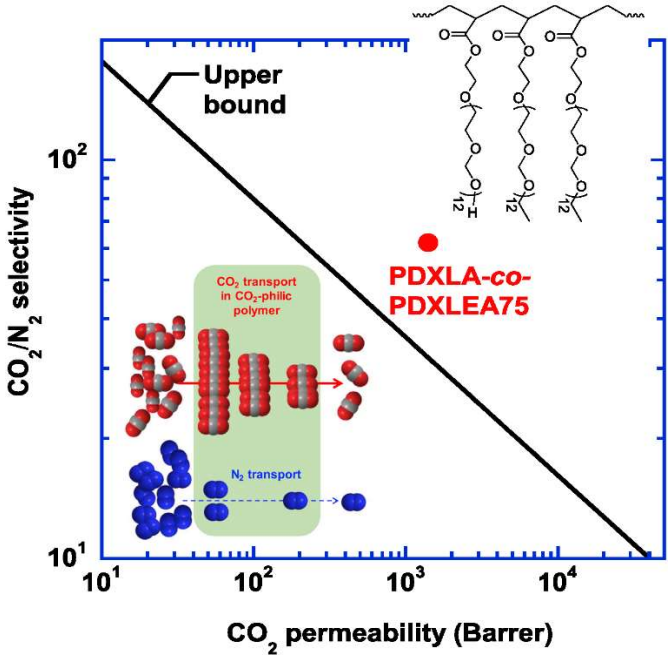

Figure 3. CO_2 permeability and CO_2/N_2 selectivity of an ether oxygen-rich poly(1,3-dioxolane). Adapted from Ref. [29] with permission from Elsevier.

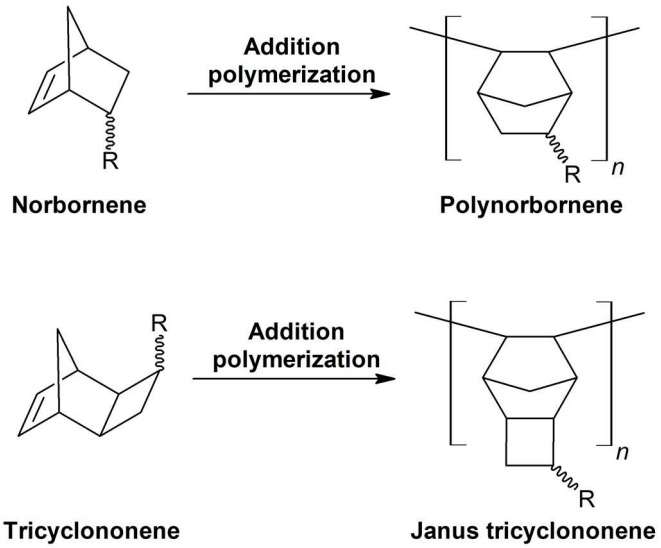

Figure 4. Vinyl-addition polymerization of norbornene and tricyclononene.

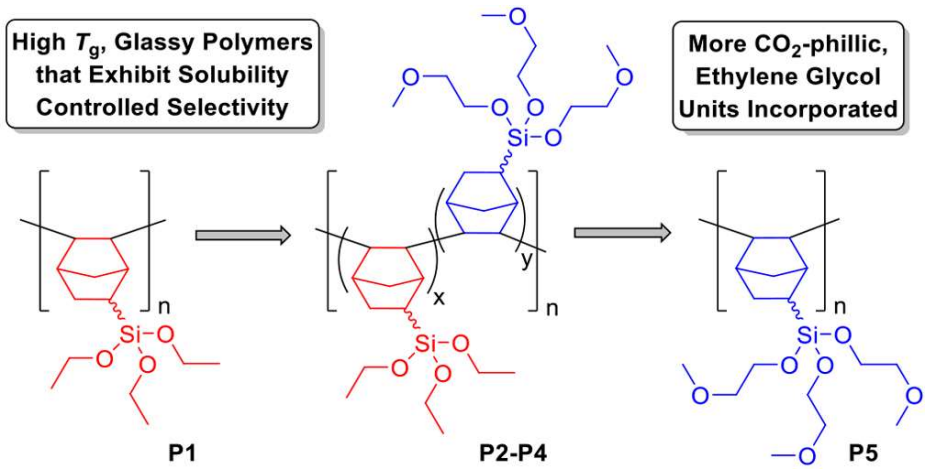

Figure 5. Polymers containing 5-triethoxysilyl-2-norbornene (red) and 5-tris(2-methoxyethoxy)-2-norbornene (blue) units. Adapted from Ref. [40] with permission from ACS.

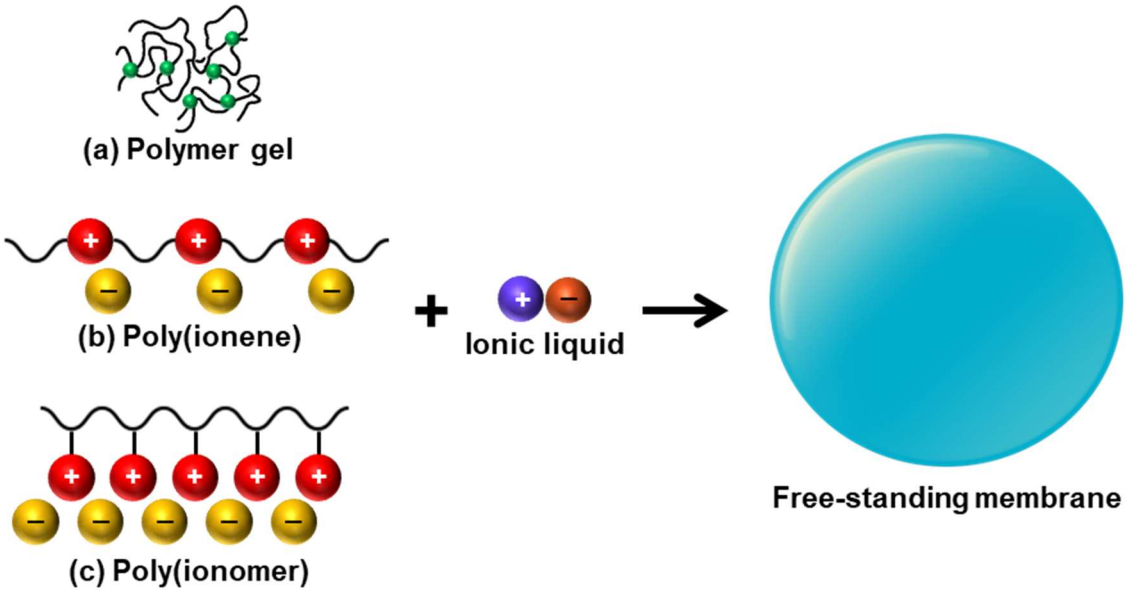

Figure 6. Representations of general formation methods of ionic liquid membranes.

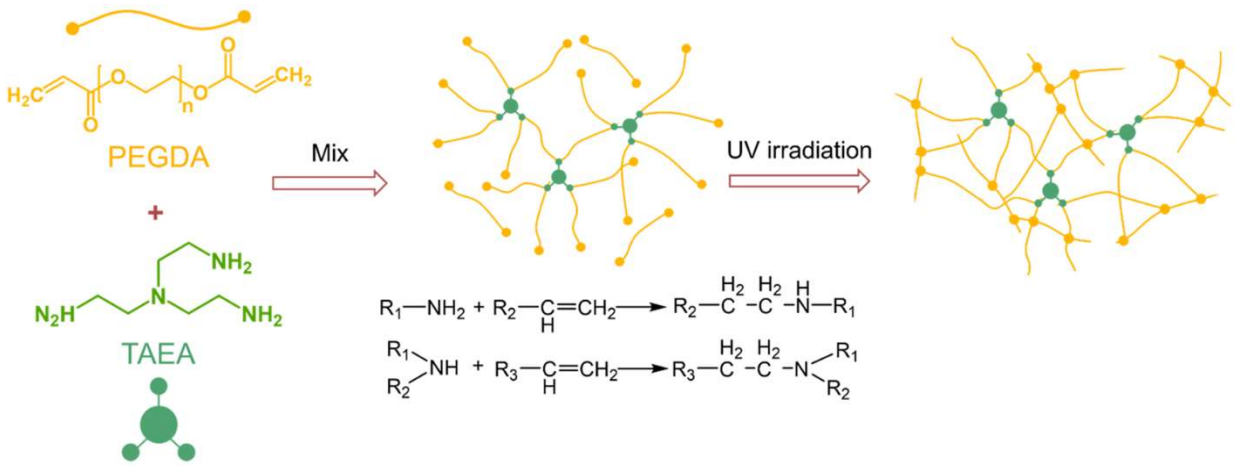

Figure 7. Schematic representation of the two-stage procedure for preparing the cross-linked tris(2-aminoethyl)amine-poly(ethylene glycol) diacrylate membrane. Adapted from Ref. [47] with permission from ACS.

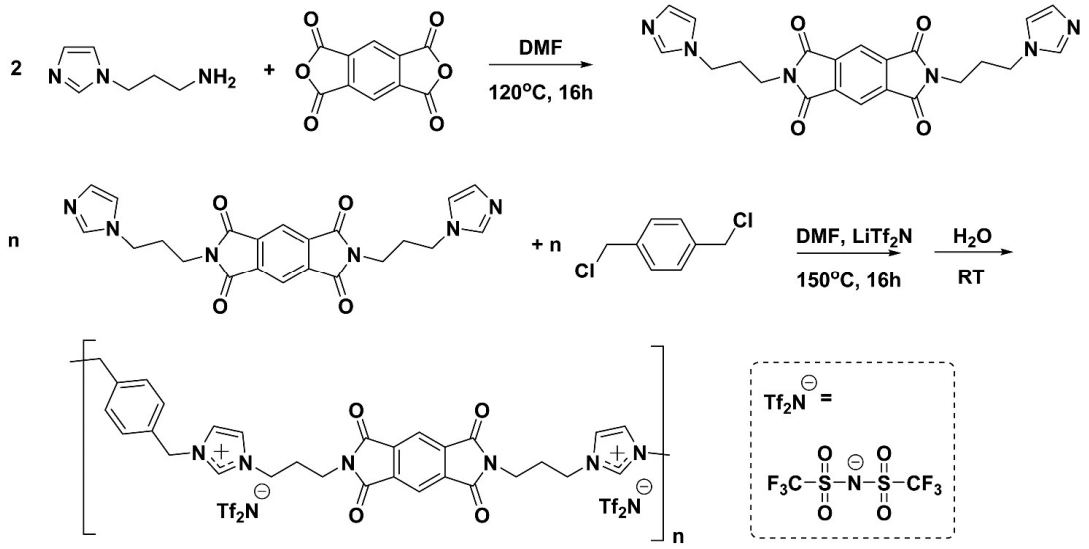

Figure 8. Synthesis of bis(imidazole) diimide monomer and ionic polyimide. Adapted from Ref. [50] with permission from ACS.

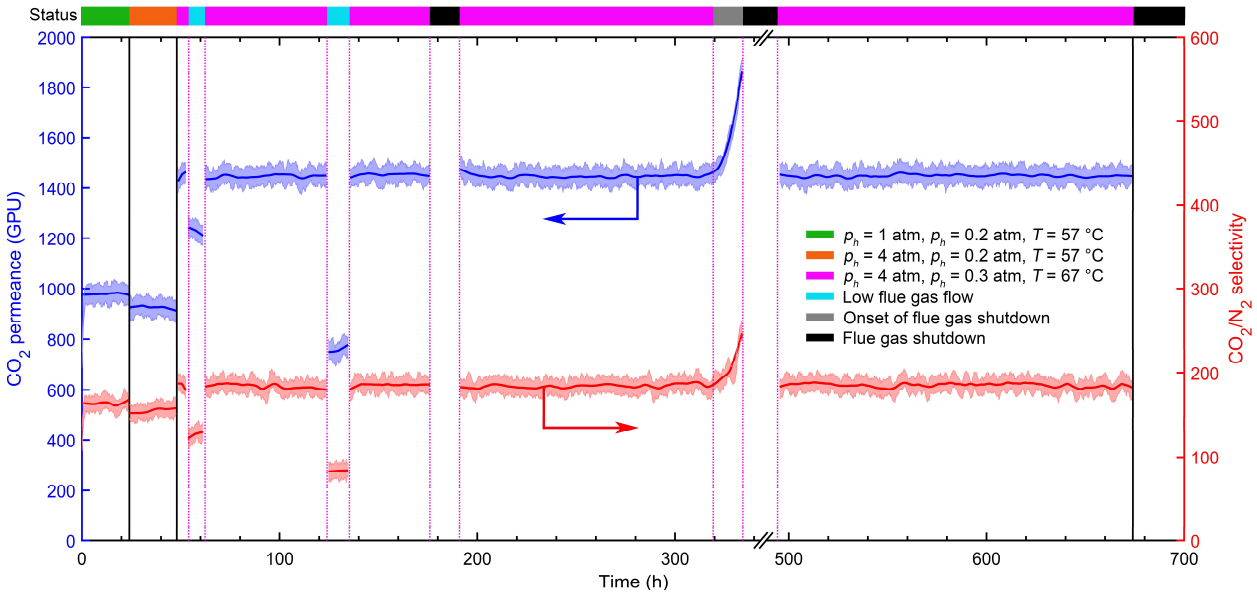

Figure 9. Stability plot of spiral-wound facilitated transport membrane module tested with actual flue gas at National Carbon Capture Center (NCCC), Alabama, U.S.A. for 500 hours. Adapted from Ref. [63] with permission from Elsevier.

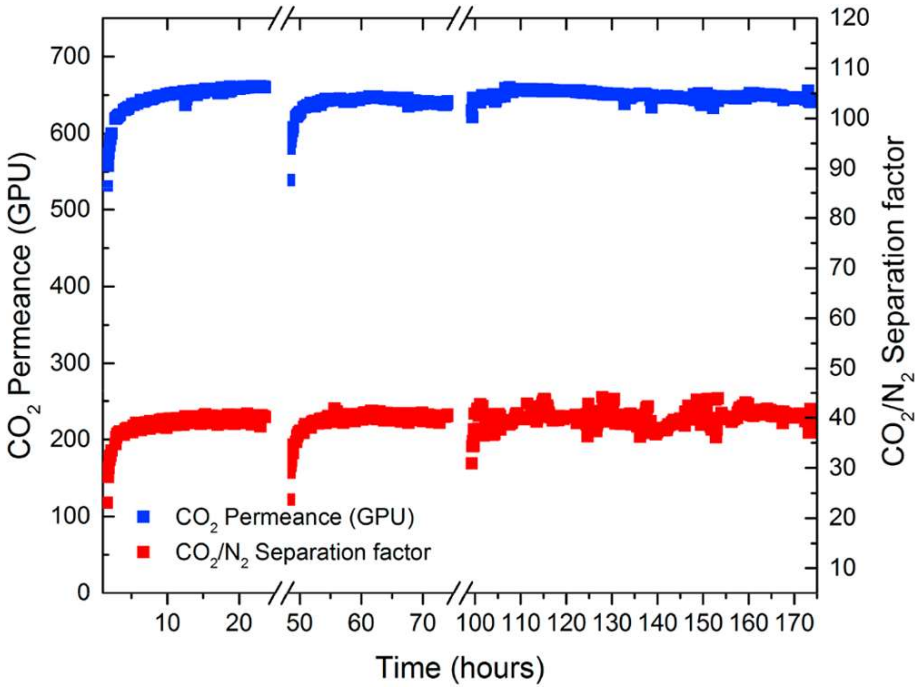

Figure 10. Permeation stability tests with forced breaks of PVA/PAA-iPr/30 wt.% PEG-decorated nanocellulose membranes measured at 35°C. Adapted from Ref. [66] with permission from ACS.

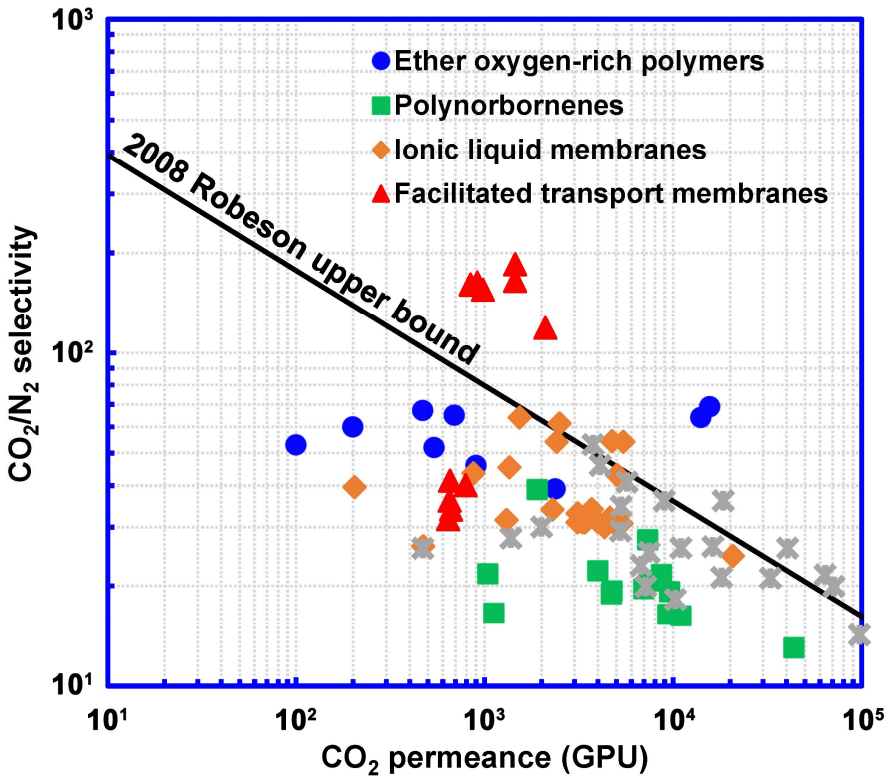

Figure 11. Transport properties of selected polymeric materials vs. 2008 Robeson upper bound at 30°C [69]. Except the data of facilitated transport membranes, all CO_2 permeance values are calculated based on the CO_2 permeability data and assuming a membrane thickness of 100 nm. Gray cross markers represent selected data summarized in our previous review paper [12].

Tables

Table 1. Physical properties of CO_2 and N_2 [16].

Gas	Kinetic diameter (Å)	Critical volume ($cm^3\ mol^{-1}$)	Critical temperature (K)	Lennard-Jones temperature (K)
CO_2	3.30	93.9	304.1	257.8
N_2	3.64	89.8	126.2	95.2

Table 2. Transport properties of selected ether oxygen-rich polymers.

Category	Material	$p(CO_2)$ (atm)	T (°C)	$P(CO_2)$ (Barrer)	α (CO_2/N_2)
Polymers derived from heterocyclic acetals	Poly(1,3-dioxolane) [29]	1	70	1400	64
	$(DXL)_{12}$-*r*-$(OM)_0A$ [31]	1	35	234	–
	$(DXL)_5$-*r*-$(OM)_2A$ [31]	1	35	208	–
	$(DXL)_6$-*r*-$(OM)_5A$ [31]	1	35	138	–
	$(DXL)_5$-*r*-$(OM)_7A$ [31]	1	35	51	–
	$(DXL)_0$-*r*-$(OM)_5A$ [31]	1	35	40	–
Copolymerization & crosslinking	$PAN_{0.6}$-*r*-$PEGMA_{0.4}$ [32]	1	25	2	52
	$PAN_{0.4}$-*r*-$PEGMA_{0.6}$ [32]	1	25	10	53
	$PAN_{0.36}$-*r*-$PEGMA_{0.64}$ [32]	1	25	20	60
	$PAN_{0.33}$-*r*-$PEGMA_{0.67}$ [32]	1	25	69	65
	PAN-*r*-PEGMA-*r*-PDMAEMA [33]	1	25	47	67.2
	PI-PEO600 [34]	3	35	54	52
	PI-PEO2000 [34]	3	35	90	46
	Pebax®/PGP-POEM [35]	1	35	237	39
	PEO-POSS-NH_2 [36]	3.5	35	1567	69

Table 3. Transport properties of selected polynorbornenes.

Category	Material	$p(CO_2)$ (atm)	T (°C)	$P(CO_2)$ (Barrer)	α (CO_2/N_2)
Polynorbornenes with alkoxy silyl pendant group	PNB-$Si(Me)_3$ [40]	1	35	4371	13
	PNB-$Si(OEt)_3$ [41]	1	35	936.6	16.4
	PNB-$Si(OEt)_2Me$ [41]	1	35	474.2	19.3
	PNB-$Si(OEt)Me_2$ [41]	1	35	470.7	18.9
	PNB-$Si(OEt)_{3(0.75)}$-$Si(OEtOMe)_{3(0.25)}$ [40]	1	35	868.8	21.6
	PNB-$Si(OEt)_{3(0.5)}$-$Si(OEtOMe)_{3(0.5)}$ [40]	1	35	733.3	27.5
	PNB-$Si(OEt)_{3(0.25)}$-$Si(OEtOMe)_{3(0.75)}$ [40]	1	35	700	19.6
	PNB-$Si(OEtOMe)_3$ [40]	1	35	745.8	20.7
Janus tricyclononenes with alkoxysilyl groups	TCN-$Si(Me)_3$ [42]	1	35	112	16.5
	TCN-$Si(OMe)_3$ [42]	1	35	190	38.8
	TCN-$Si(OEt)_3$ [42]	1	35	400	22.2
	TCN-$Si(OPr)_3$ [42]	1	35	960	19.2
	TCN-$Si(OBu)_3$ [42]	1	35	1100	16.2
Crosslinked polynorbornenes	Polyvinylnorbornene [43]	1	35	104.3	21.7

Table 4. Transport properties of selected ionic liquid membranes.

Category	Material	$p(CO_2)$ (atm)	T (°C)	$P(CO_2)$ (Barrer)	α (CO_2/N_2)
Ion-gels	TAEA-PEGDA/[bmim][BF_4] [47]	2	35	87	43.5
	TAEA-PEGDA/[bmim][PF_6] [47]	2	35	47	26.3
	TAEA-PEGDA/[bmim][TCM] [47]	2	35	135	45.3
	TAEA-PEGDA/[bmim][Tf_2N] [47]	2	35	130	31.5
	xl-PEO/[emim][Tf_2N] [48]	1	40	529	30.8
	xl-PEO/[egmim][Tf_2N] [48]	1	40	459	32
	xl-PEO/[eg_3mim][Tf_2N] [48]	1	40	370	34
	xl-PEO/[Hemim][Tf_2N] [48]	1	40	229	33.9
	PEGDA/thiosiloxane/[emim][Tf_2N] [49]	1	40	340	31
	PEGDA/thiosiloxane/[emim][DCA] [49]	1	40	240	54
	PEGDA/thiosiloxane/[N_{4111}][Tf_2N] [49]	1	40	310	33
	PEGDA/thiosiloxane/[empy][Tf_2N] [49]	1	40	330	31
	PEGDA/thiosiloxane/[bmpyrr][[Tf_2N] [49]	1	40	310	31
	Trimethylolpropane ethoxylate triacrylate/[emim][Tf_2N] [46]	1	40	395	31.2
	Ethoxylated bisphenol-A diacrylate/[emim][Tf_2N] [46]	1	40	486	30.9
Poly(ionene)s	[Im-TB(*o*)-C_{10}][Tf_2N] [51]	3	20	4.4	33.9
	Ionic polyimide/[C_4mim][Tf_2N] [50]	3	22	20.4	39.5
	[Im-OEt][Tf_2N]/[emim][Tf_2N] [52]	0.2	35	2070	24.6
Poly(ionomer)s	Sulfonated polyimide/[C_4mim][Tf_2N] [53]	1	30	431	30
	Poly([HPyr][[$C(CN)_3$]])/[C_2mim][$C(CN)_3$] [56]	1	20	542	54
	Nexar/[bmim][BF_4] [54]	1	35	153	64
	Poly([HPyr][$N(CN)_2$])/[C_2min][$C(CN)_3$] [55]	1	20	249	61.3
	Poly([HPyr][$C(CN)_3$])/[C_2min][$B(CN)_4$]	1	20	473	54.4
	Poly([HPyr][$B(CN)_4$])/[C_2min][$C(CN)_3$]	1	20	502	43.1

Table 5. Transport properties of selected facilitated transport membranes.

Category	Material	$p(CO_2)$ (atm)	T (°C)	Thickness† (μm)	P/ℓ (CO_2) (GPU)	α (CO_2/N_2)
Amine carriers	PVAm/PZ-Gly [61]	0.166	57	0.17	839	161
	PVAm/PZEA-Gly [61]	0.166	57	0.17	911	163
	PVAm/PZEA-Sar [61]	0.166	57	0.17	975	155
	PVAm/PZEA-Sar [62]	0.731	67	0.17	1450	165
	PVAm/PZEA-Sar [62]	0.708	77	0.17	2100	119
	PVAm/PZEA-Sar‡ [63]	0.102	67	0.17	1450	185
	PVA/Pro-K [64]	0.197	22	0.5	793	40.1
	PVA/Gly-K [64]	0.197	22	0.5	640	31.7
	PVA/Cys-K [64]	0.197	22	0.5	650	36
	PVA/PAA-iPr/PZEA-Sar [66]	1.48	35	0.29	652	41.3
Other carriers	PVA/Arg-K [64]	0.098	22	0.5	661	33.9
	Nanocellulose/Arg [67]	5.94	35	–	220 Barrers§	185
	PEO/CF_3CO_2K [68]	0.978	25	1.3	4650	1500

† Selective layer thickness in a thin-film composite membrane

‡ Bench-scale testing with actual flue gas

§ Only permeability data are available